

A New method for identifying possible causal relationships between CO₂, total solar irradiance and global temperature change

Knut L. Seip¹ · Øyvind Grøn¹

Received: 10 June 2015 / Accepted: 4 November 2015 / Published online: 20 November 2015
© Springer-Verlag Wien 2015

Abstract We apply a novel method based upon “before” and “after” relationships to investigate and quantify interconnections between global temperature anomaly (GTA), as response variable, and greenhouse gases (CO₂) and total solar irradiance (TSI) as candidate causal variables for the period 1880 to 2010. The most likely interpretations of our results for the 6 to 8 years cyclic components of the variables are that during the period 1929 to 1936, CO₂ significantly leads GTA. However, during the period 1960–2003, GTA apparently leads CO₂, that is, the peaks (and troughs) in GTA are in front of, and close to, the peaks (and troughs) in CO₂. For time windows outside these periods, we did not find significant before or after-relationships. An alternative interpretation is that there is a shift between short (≈ 1.5 year) and long (≈ 5 years) durations between cause and effect. Relationships between GTA and TSI suggest that “inertia” of the global sea, land, and atmosphere system leads to delays longer than half their common cycle length of about 10 years. Based on the interaction patterns between the variables GTA, CO₂, and TSI, we suggest the possibility that a new regime for how the variables interact started around 1960. From trend forms, and not considering physical mechanisms, we found that the trend in CO₂ contributes ≈ 90 %, and the trend in TSI ≈ 10 %, to the trend in GTA during the last 130 years.

Electronic supplementary material The online version of this article (doi:10.1007/s00704-015-1675-8) contains supplementary material, which is available to authorized users.

✉ Knut L. Seip
knut.lehre.seip@hioa.no

Øyvind Grøn
oyvind.gron@hioa.no

¹ Faculty for Technology, Art and Design, Oslo and Akershus University College of Applied Sciences, Pilestredet 35, POB 4 St. Olavs plass, N-0130 Oslo, Norway

1 Introduction

The global averaged combined land and ocean surface temperature has increased by about 0.65 °C to 1.06 °C over the past 133 years, the period ending in 2012 (Stocker 2014, p. 5). The warming occurred largely during two periods, between 1910 and 1940 and since the mid-1970s to about 1998. In the years 1943–1975 and 1998–2013, there are periods with non-increasing global temperature anomaly (GTA) (the hiatus periods, Meehl et al. (2014), but see Karl et al. (2015) for a possible exception of the last period). Several factors have been suggested as causal agents for the observed changes in global temperature, and a survey that separates the strength of causes into time slots are given in Ring et al. (2012). However, explaining cycle lengths and lag times have been difficult, e.g., Ray (2007), in particular for CO₂, since stores and flux from land are not well known, Stocker (2014), p. 792.

Here, we study carbon dioxide (CO₂) and total solar insolation (TSI) as candidate causal agents for changes in GTA. TSI is an exogenous variable and is a measure of the solar radiative power per unit area normal to the rays, incident on the Earth’s upper atmosphere. We examine possible causal relations in long term (1880–2014) and shorter term, multidecadal and decadal, perspectives. In the decadal and multidecadal perspective, we examine “before” and “after” relationships for (quasi-) oscillatory movements. A necessary, but not sufficient, requirement for a causal agent is that it has to come before the effect. For cyclic phenomena, this statement can be interpreted in terms of succession between peaks and troughs in the series. If the peak (or trough) of the candidate causal agent comes shortly ($< \frac{1}{2}$ cycle length) before the peak (or trough) of the effect, then this finding, together with a mechanistic model of the system, may strengthen a possible causal relationship. If the peak (or trough) in the candidate causal agent comes a long time ($> \frac{1}{2}$ cycle length) before the

effect, then we would require, if possible, reasonable intermediate mechanisms that are lagging the candidate cause, but leading the effect. Since mechanistic models may indicate that a decrease in an agent may have a causal effect, we change the sign of the causal agent so that the peaking statement can be true.

If two variables are hypothesized to show reciprocal dynamic interactions, then we believe the most probable interpretation will be that the variable that peaks (or has a trough) in front of, and close to the peak (or trough) of the other variable contributes a causative effect to the latter. However, system knowledge is required to determine the most probable interpretation. For pairs where one variable is exogenous to the system studied, like GTA and TSI (TSI exogenous), a lagging signature for the exogenous agent means that it is leading, but with a long time delay ($>1/2$ cycle length).

Leading–lagging (LL) analyses, as well as regression analyses, are also exposed to several mechanism that can cause spurious relations and interpretations. We will examine these in the discussion section.

We try to accumulate evidence to strengthen the causal links between TSI, the concentration of CO₂, and GTA. There are also other variables that contribute to changes in GTA, but they appear to be particularly strong for local or regional temperature regimes, e.g., the North Atlantic Oscillation (NAO), the Southern Oscillation Index (SOI), and the Pacific Decadal Oscillation (PDO) (Luterbacher et al. (2002), Bacastow (1976), Power and Kociuba (2011), Chylek et al. (2014 b), Finlay et al. (2015), and Meehl et al. (2011). Carbon dioxide, CO₂ may also impact NAO and PDO, e.g., Chylek et al. (2014a), pp. 125–7 by yet unknown mechanisms. The treatment of these variables is therefore outside the scope of the present study, but is included in the study program.

1.1 Trends and cycles in global changes of variables

The main objective of this study is to examine before and after relationships between candidate causal agents and global temperature change. Since there is more information available between the cyclic components of variables than between their trends, we first examine the cyclic component and thereafter the trends. We suggest that a candidate causal agent strengthens its candidature if it is (i) consistently before the effect, (ii) it does so across many cycles, and (iii) the cycles have varying cycle lengths.

We show in this study that there are variables that appear as leading factors, but that cannot have any causal effect, and thus force us to consider response times longer than half the characteristic cycle time, T . However, we only cursory try to identify possible delaying mechanisms in the present study, but believe that leading or lagging relationships between ocean water movements may offer partial explanations.

We use multiple regression methods to investigate the relationships between trends for the time series, GTA, CO₂, and TSI as they are expressed by a locally weighted polynomial regression technique, the LOESS–smoothing algorithm, SigmaPlot©.

1.2 Hypotheses

Firstly, we hypothesize that once trends are subtracted from GTA, CO₂, and TSI, CO₂ and TSI will be leading variables to GTA. Secondly, even if there are not significant LL-relationships that persist over the full data series, there may be time windows where pairs of variables have common cycles. We assume that each pair will have different time windows where the coupling is strong. Thirdly, we hypothesize that the trends of both CO₂ and TSI contribute to the trend in GTA and CO₂ more than TSI.

The paper is organized as follows. In Section 2, we present the materials, in Section 3, we present three major methods used in the analysis: (i) pretreatment of the data, (ii) the method for quantifying leading-lagging relationships, and (iii) uncertainty estimates. Section 4 presents the results and in Section 5, we discuss the results. Section 6 concludes.

2 Materials

We examine three time series, the global temperature anomaly (GTA), the greenhouse gas (CO₂), and total solar irradiance (TSI). The raw data for the three series are shown in Fig. 1a. For each of the series, we report (i) the sources we have used for the data, (ii) possible errors reported for the data, (iii) characteristic cycles that have been found in the data and that are reported in the literature, and (iv) simplistic observations of cycle times by estimating period and cycle lengths for the detrended GTA, CO₂, and TSI using crossing points with the zero line. A similar crossing point method was used by Gao et al. (2015).

Parts of the three series are more uncertain than other parts. In particular, reconstructions of old parts may be uncertain with respect to the exact dating of the values. Chylek et al. (2014 a) limit their analysis to the period 1910–2012 to avoid observational uncertainty in the early data, whereas we include data from 1880. However, the results related to the period 1880–1920 do not alter our main results.

The global temperature series We use the GISS Global land–ocean temperature Index in 0.01 degrees Celsius from NASA’s Goddard institute for space studies, NASA (GISTEMP) (2014). The data are from the website http://data.giss.nasa.gov/gistemp/tabledata_v3/GLB.Ts+dSST.txt. The series are updated every month and may change within their margin of error (R. Ruedy personal communication).

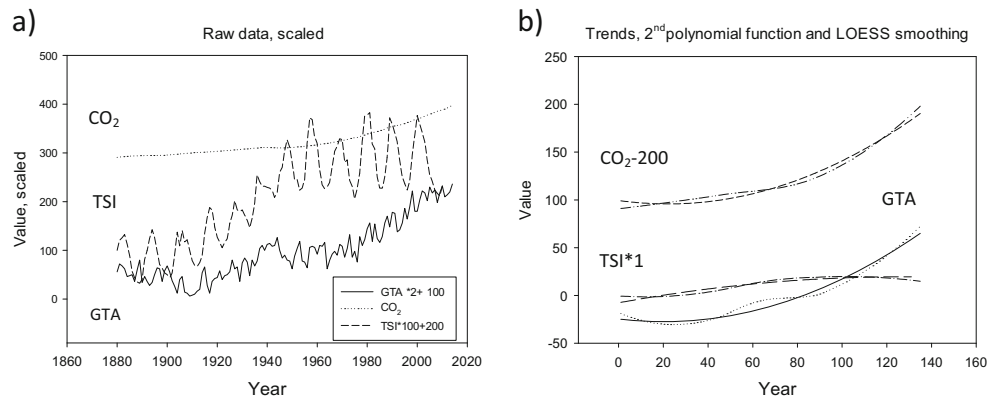


Fig. 1 Time series used in the present study. **a** Raw data for CO₂, concentrations, combined land-surface air, and sea-surface water temperature anomalies (*GTA*) (deviations from 1951 to 1980 mean, in 0.01 °C), and total solar irradiance (*TSI*) as reported by NOAA. **b**

There were certain changes in the sampling procedure for *GTA* in 1945, shifting the temperatures systematically down, Wu et al. (2011a). For the *GTA* series Zhen-Shan and Xian (2007) and Mazzarella and Scafetta (2012) both found that during the period 1880 to 2009, *GTA* has dominating cycle lengths of 6–8, 20, and 60 years. Keeling and Whorf (1997), p. 8327 found cycle lengths of 6 years in global air temperature and White and Cayan (1998) found 20 to 23 years periods in sea surface temperatures. Zhen-Shan and Xian (2007) and Kjeldseth-Moe and Wedenmeyer-Böhm (2009) all found cycle times of 8, 20, and 60 years in the *GTA* series. We found for the period 1880–2009 17 cycles for *GTA*, with an average length of 6.8 ± 4.0 years (range 3–17) superimposed on a low-frequency 60-year cycle. In addition, we cursory examine a new *GTA* series reported in Karl et al. (2015). The data can be found on the web site: <http://www.sciencemag.org/content/348/6242/1469.abstract?keytype=ref&siteid=sci&ijkey=.1.kxQb89CJjY>

The greenhouse gas variable, CO₂ We use the global-mean carbon dioxide (CO₂) values as ppm supplied by (NASA (GHG) 2014) and NOAA retrieving data from the web sites: <http://data.giss.nasa.gov/modelforce/ghgases/GHG.1850-2000.txt> and ftp://afp.cmdl.noaa.gov/products/trends/co2/co2_annmean_gl.txt. The NASA list of greenhouse gases also include other gases, N₂O, CH₄, CFC-11, CFC-12, and others, but neither contribute more than ≈ 1 % of CO₂ on the average, and combining contributions are complex. The year-to-year data for CO₂ are uncertain before 1958 since they were based on indirect measurements.

Total solar irradiance TSI has the unit W m^{-2} as defined by SORCE (2015). The data were taken from the website <http://data.giss.nasa.gov/modelforce/RadF.txt>. The TSI data were uncertain until the use of satellites in 1979 when direct measurements above the earth's atmosphere became feasible

Quadratic and LOESS trends for *GTA*, CO₂, and TSI. Quadratic trends are smooth, LOESS trends are wiggling. Equations for quadratic trends are shown in the text

(Zhou and Tung 2010, p. 3234). According to Frohlich (2009), there is a declining trend in the TSI during the last decade, and in our TSI data we find that there is a quadratic trend spanning our study period of 131 years. We found 10 cycles for TSI with an average length of 11.1 ± 1.2 years (range 10–13 years). However, the power spectral density algorithm identified the 22 years Gnevyshev–Ohl cycles, probably based on alternating blunt and short and sharp and tall peaks. In addition, we cursory examine a new revised series for total sunspot numbers reported in Clette et al. (2014). The data can be found on the web site: <http://www.sidc.be/silso/>

3 Methods

In this section, we first describe pretreatment of our data. Thereafter, we describe a novel method for quantifying leading and lagging relationships. Thirdly, we describe our attribution method and lastly the method used to estimate uncertainty levels. Principal component analysis (PCA) was made in Unscrambler © and LOESS smoothing in and Power spectral analysis in SigmaPlot©.

3.1 Data pretreatment

We use the data in their native units except for TSI that are given in W m^{-2} . Time series will often represent a superposition of several variables where each has its own characteristics. A major task is therefore to distinguish the different trends and cycles that express the effect of each variable on *GTA*. The choice of method depends both upon the underlying mechanisms that generate the pattern in the series and upon the purpose of the study. The Hodric-Prescott filter has for example parameters that allow the user to focus on cycle lengths of interest (Cooley and Prescott 1995). Merging cycles that are imposed on a system, e.g., seasonal driving forces, and

cycles that are generated by interaction dynamics, may result in complex patterns that are functions of the relative contributions of the two driving forces (Seip and Pleym 2000). Foster and Rahmstorf (2011): period 1979–2011, Zhou and Tung (2010): period 1854–2007, and Karl et al. (2015): different periods 1950–2014 evaluate linear trends. Wu et al. (2011a, b) and Ring et al. (2012) discuss non-linear trends and Munk et al. (2002) and Ray (2007) suggest that high and low beat frequencies between cycles with close frequencies may play a role.

Identifying long-term trends and residuals We identify the long-term trend from the three time series GTA, CO₂, and TSI and by dividing the series into a skeleton described by a second-order polynomial equation and its residuals. All variables were centered and normalized to unit standard deviation except that we regressed the original data with GTA as dependent variable and CO₂ and TSI as independent variables also in their original units. Centering and normalizing to unit standard deviation is also called a Z-transform (Finlay et al. 2015). The term “trend” is thus not limited to a significant non-zero linear slope, but we require it to cover the whole study period, i.e., secular trends as in, e.g. Wu et al. (2011a, b).

The residuals will often have a cyclic character and thus show serial correlation. By removing the trends, we may also remove very long cycles, and we distort cycle lengths. In particular, if two cyclic series are to be compared, we may distort cycle lengths differently, and also distort the phase shift between the two cycles. Often, series that are to be detrended do not comply with the statistical assumptions required to calculate true probability values, but we use the probability values conservatively when we report regressions not to be significant. We approximate the secular trend with both quadratic functions and the LOESS locally weighted algorithm for the whole period 1880 to 2014.

3.2 Quantifying running average phase shifts relations for pairs of variables

Our main contribution is to extract running average phase shifts and leading and lagging properties (i.e., the sign of the phase shift relative to a fixed “first-last” sequence) of the paired time series by a novel method. The method gives quantitative expressions for leading and lagging relations between paired (quasi-) cyclic time series. The method also quantifies cycle lengths and time lags. An application to a synthetic set of data is given in Supplementary information 1.

We here present the new method (henceforth called the LL-method) for quantifying possible causal relationships between a pair of observed variables, $x(t)$ and $y(t)$.

In order to facilitate description of the method, we first think of the peak-trough sequence of the observations as a pair of “observed” sine functions that both have period 2π , but have a difference in phase, τ , relative to each other,

$$x = \sin(\omega t) ; y = \sin(\omega t + \tau) \tag{1}$$

Let x be plotted on the x -axis of a phase plot and y on the y -axis. Hence Eq. (1) may be interpreted as a parametric description of Lissajous figures (Fig. 2). We shall illustrate the LL-method by referring to the Lissajous curve where $\tau \in [-2\pi, 0]$.

We can then describe the relationship between the two sine functions by two parameters. The first (i) is a rotational direction expressed by the sign of the rotation angle $V_{i-1,i,i+1}$ for the trajectories in the phase plot. The second (ii) is the regression slope or the β -coefficient of the linear regression for the scatter plots of “sampled” sine functions.

We shall now explain how the direction of rotation of the trajectories in the phase portrait expresses whether an alternative series, y , is before (leading) or after (lagging) a target series x . Four examples are shown in Fig. 3.

Let us first show that Eq. (1) is a parametric description of the ellipses in Fig. 3. Using the formulae for sinus to the sum of two angles and the identity $\cos(\omega t) = \pm \sqrt{1 - \sin^2(\omega t)}$, we have

$$y = x \cos \tau \pm \sqrt{1 - x^2} \sin \tau \tag{2}$$

which may be written

$$y^2 - 2xy \cos \tau + x^2 = 1 \tag{3}$$

Rotating the coordinate system by an angle $\pi/4$ so that $x \rightarrow (x' - y')/\sqrt{2}$, $y \rightarrow (x' + y')/\sqrt{2}$ we obtain,

$$(1 - \cos \tau)x'^2 + (1 + \cos \tau)y'^2 = 1 \tag{4}$$

This is the equations of the Lissajous ellipses in Figs. 2 and 3.

Rotational directions We shall now consider the relation between the parameter τ and whether x is leading relatively to y . In order to obtain a simple illustration, we chose $\tau = -\pi/4$. Then, we have the situation shown in Fig. 3 right upper and lower panels.

In this study, we need to obtain values for the angle θ between two consecutive vectors \mathbf{v}_1 and \mathbf{v}_2 in the range $-\pi$ to π to distinguish clockwise and counterclockwise rotations. Because the cosine function is monotonously, increasing only in the domain 0 to π , the function arc \cos is only defined on the domain -1 to $+1$ and obtains values in the range 0 to π . Let \mathbf{v}_1 and \mathbf{v}_2 be consecutive vectors in the phase space formed by

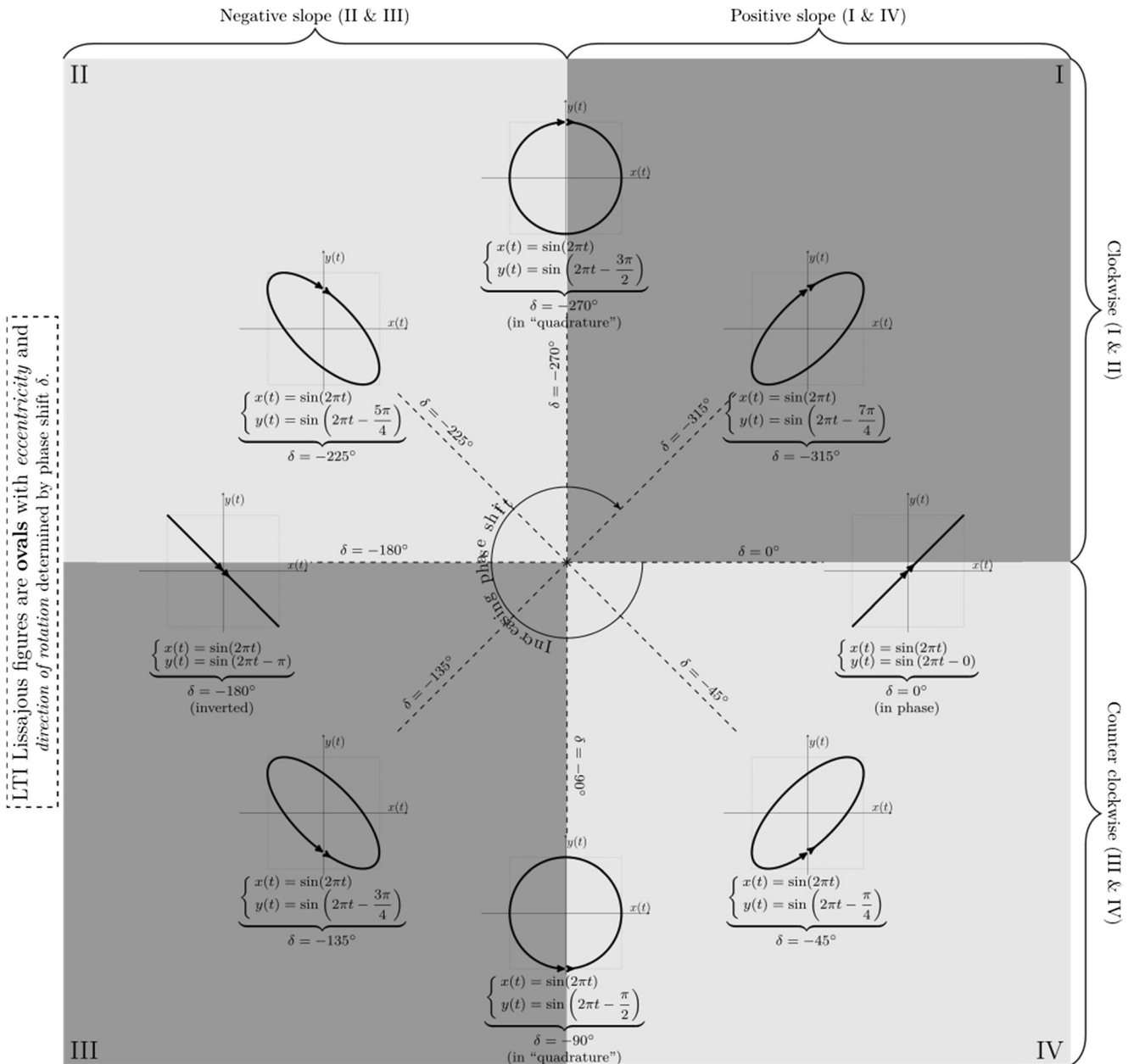


Fig. 2 Lissajous curves. From Wikipedia, http://en.wikipedia.org/wiki/Lissajous_curve

three consecutive observations. By introducing the sign of the cross product between \mathbf{v}_1 and \mathbf{v}_2 , we extend the range for the angle, θ , between the vectors to $\theta \in [-\pi, \pi]$ as required. The formula thus gets the form,¹

$$\theta = \text{sign}(\mathbf{v}_1 \times \mathbf{v}_2) \cdot \text{Arccos}\left(\frac{\mathbf{v}_1 \cdot \mathbf{v}_2}{\|\mathbf{v}_1\| \|\mathbf{v}_2\|}\right) \quad (5)$$

¹ It can be implemented in Excel format: with $v_1 = (A1,A2,A3)$ and $v_2 = (B1,B2,B3)$ in an Excel spread sheet, the angle is calculated by pasting the following Excel expression into C2: = SIGN((A2-A1)*(B3-B2)-(B2-B1)*(A3-A2))*ACOS(((A2-A1)*(A3-A2) + (B2-B1)*(B3-B2))/(SQRT((A2-A1)² + (B2-B1)²)*SQRT((A3-A2)² + (B3-B2)²))).

In order to find the relation between the phase shift τ and the rotational direction marked with arrows on the ellipses in Fig. 3, we may think of the ellipse as the path of a planet with a position given geometrically in Eq. 1. The velocity vector is

$$\mathbf{v} = \omega \cos \omega t \mathbf{e}_x + \omega \cos(\omega t + \tau) \mathbf{e}_y \quad (6)$$

The direction of rotation is given by the vorticity of the “velocity field,”

$$\nabla \times \mathbf{v} = \left(\frac{\partial v^y}{\partial x} - \frac{\partial v^x}{\partial y} \right) \mathbf{e}_z. \quad (7)$$

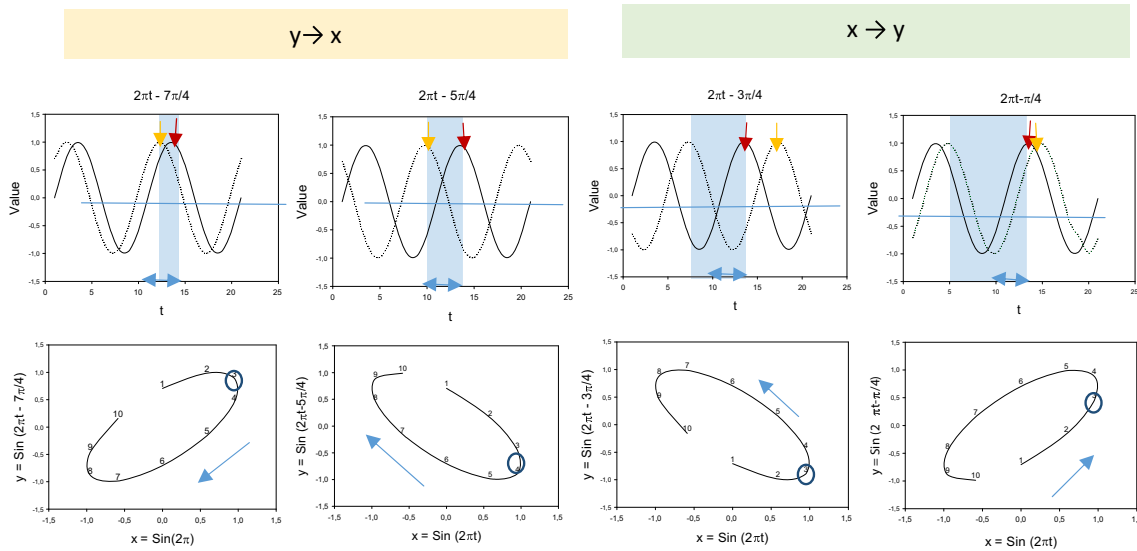


Fig. 3 The leading-lagging method. Two sine time series plotted as time series plot (upper panels, 20 observations) and as phase plot (lower panels, first 10 observations). The target sine, $\sin(2\pi t + \tau)$, in bold in the upper panels is fixed with $\tau = 0$, the alternative sine is shifted with τ assigned values: $-7\pi/4, -5\pi/4, -3\pi/4, -\pi/4$. In the phase plot, the sines that are shifted less than π (blue rectangles in the two left panels) shows a clockwise rotation. Sines that are shifted more than π (blue rectangles in the two right panels) shows counterclockwise rotation (positive per

definition). *Upper panels:* the red and orange arrows point at neighboring peaks. The double arrow at the bottom shows the distance that corresponds to π . *Lower panel:* the arrow shows rotational directions. The circled number shows the position of the first peak in the target series. The regression coefficients for the scatterplots corresponding to phase plots are from left to right $+0.707, -0.707, -0.707,$ and $+0.707$. The angles in the phase plot range from 0.28 to 1.3 rad and the sum for each period is 6.28 rad

Using again the equation for the sine of the sum of two angles, we have

$$\cos \omega t = \frac{y - x \cos \tau}{\sin \tau} \tag{8}$$

Hence, we can write

$$v^x = \frac{y - x \cos \tau}{\sin \tau} \omega, \quad v^y = \frac{y - x \cos \tau}{\sin \tau} \omega \cos \tau - x \omega \sin \tau \tag{9}$$

This gives

$$\nabla \times v = -\frac{1 - \cos \tau}{\sin \tau} \omega \mathbf{e}_z, \tag{10}$$

which is the relationship between the rotational direction and the phase shift τ . With the chosen range of τ the formula says that the rotational direction changes at $\tau = -\pi$.

Look now at the Lissajous ellipses in Figs. 2 and 3. The pattern in quadrant I emerges if the second sine is shifted by $\tau \in \langle -2\pi, -3\pi/2 \rangle$ relative to the first; the pattern in quadrant II emerges if the shift is $\tau \in \langle -3\pi/2, -\pi \rangle$; the pattern in quadrant III emerges if the shift is $\tau \in \langle -\pi, -\pi/2 \rangle$, and the pattern in quadrant IV emerges if the shift is $\tau \in \langle -\pi/2, 0 \rangle$. Furthermore, the patterns in quadrants I and II have clockwise rotations, and the patterns in quadrants III and IV have counterclockwise rotations. Thus, there is clockwise rotations for $\tau \in \langle -2\pi, -\pi \rangle$ and counterclockwise rotations for $\tau \in \langle -\pi, 0 \rangle$.

Consider now the curves of $x(t)$ and $y(t)$ as given in Eq. (1). Plotting these curves, we see that the variable on the

y -axis peaks before the variable on the x -axis, i.e., y leads x , if $\tau \in [-2\pi, -\pi]$, i.e., if there is clockwise rotation. On the other hand, the variable on the y -axis peaks after the variable on the x -axis, i.e., y lags x , if $\tau \in [-\pi, 0]$, i.e., if there is counterclockwise rotation. Hence, clockwise rotation means that y is a leading variable relative to x , and counterclockwise rotation means that y is a lagging variable relative to x . The leading-lagging relationship is then consistent with the normal use of LL-relationships in economics, and with an intuitive understanding of LL-relations.

Our argumentation has been restricted to the 2π domain. However, a lagging relationship can also be interpreted as a leading relationship with long leading time ($> 1/2$ cycle time).

The strength, LL, of the mechanisms that cause two noisy variables to either rotate clockwise or counterclockwise in a phase portrait is measured by the number of positive rotations (counterclockwise rotations by convention) minus the number of negative rotations, relative to the total number of rotations over a certain period, in this study, 9 years.

$$LL = (N_{\text{pos}} - N_{\text{neg}}) / (N_{\text{pos}} + N_{\text{neg}}) \tag{11}$$

The LL-strength obtains a high/low value when one variable is consistently leading or lagging another. However, with varying cycle lengths, the two series have to change cycle lengths in concert for the measure to obtain a consistent high/low value. We consider common cycle lengths as supporting factors for a causal relationship between two

variables. We use the nomenclature: $LL(x, y) = [-1, 1]$ for leading-lagging strength: $LL(x, y) < 0$ implies that y leads x , $y \rightarrow x$; $LL(x, y) > 0$ implies that x leads y , $x \rightarrow y$.

The cycle length, CL , of two paired series that have been shown to interact can be approximated as:

$$CL = n \times 2\pi / (\sum_2^{n-1} V_{i-1,i,i+1}) \quad (12)$$

For sampled perfect sine functions, Eq. (12) gives very closely the design length, 2π , of the sine functions, and the error is only affected by the sampling frequency, (see supplementary information 1). The cycle times we identify are based on full rotations in the phase plots for the paired time series. If the period that gives consistent cycles in one direction does not allow a full cycle to be completed, the estimate of cycle time may be biased towards short or long cycle times and is only shown as a guiding estimate for a probable cycle time.

Time lags, TL , the regression slopes, s , or the β -coefficients will for cyclic series give information on the shift, or time lag, between the series. For a linear regression applied to paired time series that are normalized to unit standard deviation, the regression coefficient, r , and the β -coefficient will be identical. If the two series co-vary exactly, their regression coefficient will be 1, and the time lag 0. If they are displaced half a cycle length, the series are counter-cyclic, and the correlation coefficient is $r = -1$. Lead or lag times, TL , are estimated from the correlation coefficient, r , for sequences of five observations, $TL(5)$. With λ as cycle length, an expression for the phase shift between two cyclic series can be approximated by:

$$TL \approx \lambda/2 \times (\pi/2 - \text{Arcsine}(r)) \quad (13)$$

3.3 Smoothing

We smooth the curves employing the LOESS standard smoothing algorithms. The smoothing algorithm has two variables. The first one, f , shows how large fraction of the series is used for calculating the running average. The second one, p , is the order of the polynomial function used to make interpolations. We always use $p = 2$. For calculation of LL-relationships, we use the detrended data without smoothing. To emphasize patterns in the figures showing rotational angles, we smooth the raw data, $f = 0.3$, $p = 2$, and use the smoothed data to summarize results with principal component analysis, PCA. If there are two or more cyclic series superimposed, we smooth the original series and apply the LL-strength method to the smoothed series. Since both series contain information about their common cyclic properties, we used the LL-strength values as a “stop” criterion for an algorithm that increasingly smooths the series. Alternatives for

distinguishing superimposed cycles for single series are shown in, e.g., Wu et al. (2011a, b). We did not smooth the series to remove noise, but this is an option.

3.4 Uncertainty estimates

To find an expression for the uncertainty in our estimates, we ran Monte Carlo simulations on two paired uniformly random series of $n = 10, 20, 30$, “observations,” collected $j = 10, 20, 40, 80$, and 160 replicates from each, and found the 95 % confidence interval for LL-strength as the asymptotic value for an increasing number of replicates (we used $j = 1000$). It became ± 0.19 for $n = 10$ and then decreased to ± 0.10 for $n \geq 20$. Autocorrelated noise gives an enhanced estimate of LL-strength. In the present study, we calculate running averages of the LL-strength over periods of 9 years. We treat the periods as showing significant LL-strength if $LL < -0.32$ or $LL > +0.32$. To our knowledge, there is no established significance test for this method. When we calculate cycle lengths, very small angles may contribute very long cycle lengths (the formulae for cycle lengths has the form $\lambda \approx 1/V$), therefore we exempted angles < 0.12 rad. Very large angles ≈ 1.50 rad may correspond to spikes rather than cycles and were therefore exempted. All calculations were made in Excel and with SigmaPlot 11©.

4 Results

We first present the results of our detrending procedures; secondly, we present the phase shifts and the leading and lagging relationships between the cyclic components of the variables; and lastly, we present the attribution results for secular trends. The phase shifts as well as the leading-lagging relations for the cyclic properties of the paired series are here quantified, but it will often be possible to see corresponding patterns in the series themselves by comparing peaks or troughs in the paired series. In the following, we present results for each of the three pairs separately. The results are presented in three figures with 4 or 6 panels. Panels (a) show the detrended series 1880 to about 2014, (the TSI series only extend to 2010) and a moving average β -coefficient (or slope) for the paired series. Panels (b) show the angles, V , for the trajectories in the phase plots of the pairs. The angles can be negative, showing clockwise rotations, or positive, showing counterclockwise rotations. Panels (c) show cycle times and phase shifts during periods where there are persistent and significant, $p < 0.05$, rotations of the trajectories in one direction. Regression lines suggest how cycle times and phase shifts may change with time. Panels (d) show an example of rotational trajectories during periods with persistent rotations. In Fig. 4, we have added two additional panels, (e) and (f), showing results for strongly smoothed detrended series for GTA and CO₂. With the strong

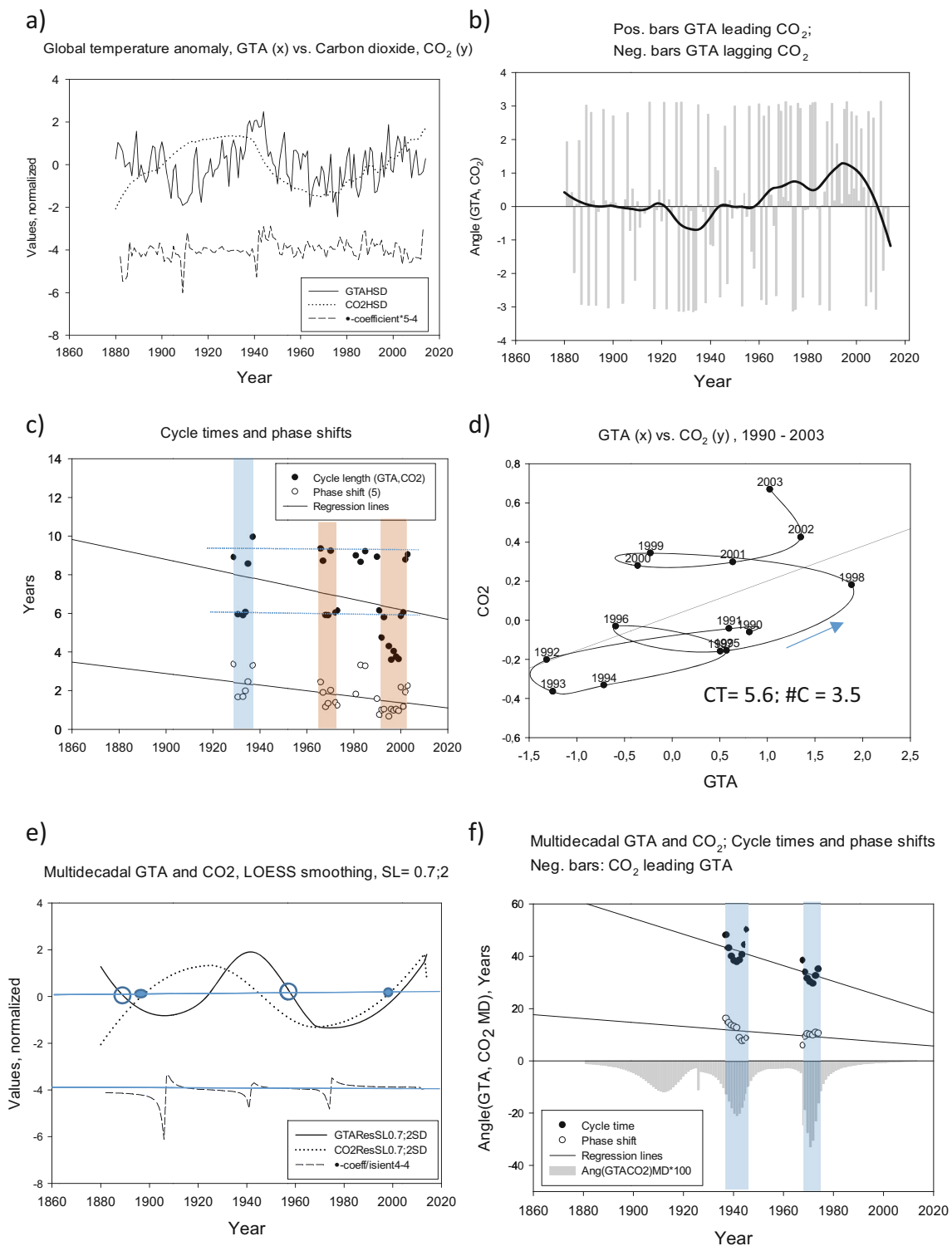


Fig. 4 Global temperature anomaly (GTA) versus carbon dioxide (CO₂). **a** Time series for CO₂ (dotted line), and global temperature anomaly, GTA (full line), lower line shows β -coefficient. Period 1880 to 2014. **b** Leading-lagging relationships between GTA and CO₂. Positive bars shows that GTA is leading CO₂ and negative bars show that GTA is lagging CO₂. The full line show smoothed trends in the LL-relationship (LOESS, $f = 0.3$, $p = 2$). **c** Running average cycle times (filled circles, $n = 9$) and phase shifts (open circles, $n = 5$) when both are significant, $p < 0.05$. CT cycle time in years, $\#C$ number of cycles during significant

period. **d** Phase diagram with GTA, (x -axis) and CO₂ (y -axis) for the years 1990 to 2003. **e** GTA and CO₂ strongly smoothed (LOESS $f = 0.7$, $p = 2$) to identify multidecadal cycles and their relationships. Open circles visually identify cycle length for GTA. Filled circles visually identify cycle length for CO₂. Lower line running average β -coefficient. **f** Leading-lagging relationships between GTA and CO₂ as multidecadal cycles, (as bars). Cycle times and phase shifts as filled and open dots respectively

smoothing, we try to capture common multidecadal trends for GTA and CO₂.

4.1 Global temperature anomaly versus carbon dioxide

We have examined the patterns of the rotational angles $V_{i-1, i+i-1}$ for GTA versus CO₂ as one moves from 1880 to 2014. The gray bars in Fig. 4b show that LL-relationships are volatile. To better see the general patterns in the bars, we have smoothed the angle data (SigmaPlot 11, 2D LOESS smoothing with $f = 0.3$ and $p = 2$). Figure 4b shows that during the period 1929 to 1936, CO₂ leads GTA, but after about 1966, GTA is leading CO₂. Figure 4c shows that the cycle length is around 7 years and the lag time between GTA and CO₂ is about 1.5 years. However, both the cycle time and the lag times appear to decrease towards the last decades, (n.s.). Alternatively, the pattern in Fig. 4c may be interpreted as reflecting both a 6-year cycle and a 10-year cycle. Figure 4d shows GTA plotted on the x -axis and CO₂ plotted on the y -axis during the period 1990 to 2003. The trajectories show a counterclockwise rotation indicating that GTA is a leading variable to CO₂.

Multidecadal cycles From Fig. 4a is seen that GTA and CO₂ have visually recognizable cycles on multidecadal scales in addition to the (quasi-) cycles on shorter time scales, e.g., DelSole et al. (2011), Wu et al. (2011a), and Gao et al. (2015). We identified relationships between the multidecadal patterns by smoothing both series strongly (LOESS, $f = 0.7$; $p = 2$, Fig. 4e) and thereafter applied the LL-strength method to the smoothed data. Visually, there appears to be two distinct periods for these multidecadal series, one from about 1880 to 1960, where the two series are shifted relative to each other and the GTA-series show a cycle time of about 60 years. The other extends from about 1960 to 2014; here, the two series are much closer to each other, and the cycle times are difficult to identify. We found two time windows where CO₂ was a significant leading variable to GTA: 1937–1945 and 1968–1974. The cycle time shown on the figure only allowed cycle lengths of $\frac{1}{4}$ cycle, thus making the estimates biased and uncertain. The general trend was that the multidecadal component of CO₂ was a leading variable to the multidecadal trend in GTA (all bars are negative).

4.2 Global temperature anomaly versus total solar irradiance

Figure 5a shows that the two series for GTA and TSI are strongly cyclic on decadal or shorter time scales. Figures 5c show that there are four periods where we obtain significant relations. In two additional periods, parts of the cycles include spikes that do not contribute to a regular cycle. Segments of leading relations can also be identified in other short periods,

$n < 3$. Since TSI is an exogenous variable, the interpretation is that TSI appears to lead GTA with both short and long time lags, that is with time lags of 3–4 years and time lags of 7–8 years. The cycle times were 11 to 12 years for the two cycles that were sampled for one cycle period, 1989–1904 and 1952–1961. During the first period, the main cyclic rotation was clockwise, but with a few counterclockwise turns.

4.3 Carbon dioxide versus total solar irradiance

Figure 6a shows detrended and normalized values for CO₂ and TSI. There are significant long and short leading relationships between TSI and CO₂ only after about 1960, Fig. 6c. During the 3 years 1964–1966, CO₂ is lagging TSI with a short delay, but during the two following periods, together about 20 years, 1987–2003, TSI is leading CO₂ with a long delay. Figure 6c shows that the cycle times, CT, are 9 to 12 years with the short lag time lags, or phase shifts, PS, in the range 1.6 to 3.3 years. The long time lags, CT–PS, is thus in the range 7 to 9 years. The rotational properties of CO₂ (x -axis) and TSI (y -axis) for the period 1987 to 2003 are shown in Fig. 6d. Since CO₂ was increasing during this period, we detrended and then normalized the data for 1960 to 2003. The rotation 1987 to 2003 is largely counterclockwise, showing positive rotations. This means that TSI is a leading variable to CO₂ with long time lag ≈ 7 –9 years. Some details are shown in Supplementary material 2.

4.4 Comparing interaction patterns

We now have three sets of moving average interaction patterns, the pairs GTA versus CO₂, TSI versus GTA, and TSI versus CO₂. To investigate if the interaction patterns have common features, we applied principal component analysis to the smoothed LL-relations (the angles) as they are depicted in panels (b) of Figs. 4, 5, and 6. However, since there seems to be a turning point around 1955 for many of the variables, e.g., in the zonal mean multidecadal variations of land surface air temperature, Gao et al. (2015), p. 364, as well as in anthropogenic greenhouse gases and aerosols, Chylek et al. (2014 a), p. 121, we divided the time series into two subsets at 1955 for ease of comparison. Figure 7a shows that during the first period 1880 to 1955, the LL-relationships LL (GTA, CO₂) and LL (TSI, GTA) are correlated, but the LL-relationship LL (TSI, CO₂) is independent from these (the arrow from the origin shows an approximately right angle to the arrow to the first two). The score plot shows no clear pattern through time. During the last period 1956 to present, it is the LL-relationships LL (CO₂, GTA) and LL (TSI, CO₂) that are correlated, whereas the relationship LL (TSI, GTA) is independent from the two former. Furthermore, the scores (Fig. 7d) suggest that the LL-relationships change systematically through time. The years 1965, 1987, and 1994 can be

Fig. 5 Global temperature anomaly (*GTA*) versus total solar irradiance (*TSI*). **a** Time series for *GTA* (*dotted line*), and *TSI* (*full line*), and *lower line* shows β -coefficient. Period 1880 to 2010. *H* detrended, *SD* normalized to unit standard deviation. **b** Short and long leading times for *TSI* on *GTA*. *Positive bars* shows that *TSI* is leading *GTA* with a long time delay, PS_{long} ($>1/2$ cycle time, *CT*; i.e., $CT-PS_{short}$) and *negative bars* show that *TSI* is leading *GTA* with short time delay. The *full line* show smoothed trends in the LL-relationship (LOESS, $f=0.3, p=2$). **c** Running average cycle times (*CT*, *filled circles*, $n=9$) and phase shifts (*PS*, *open circles*, $n=5$) when both are significant, $p < 0.05$. **d** Phase diagram with *GTA* (*x-axis*) and *TSI* (*y-axis*) for the years 1889 to 1904. Further details in text to Fig. 4

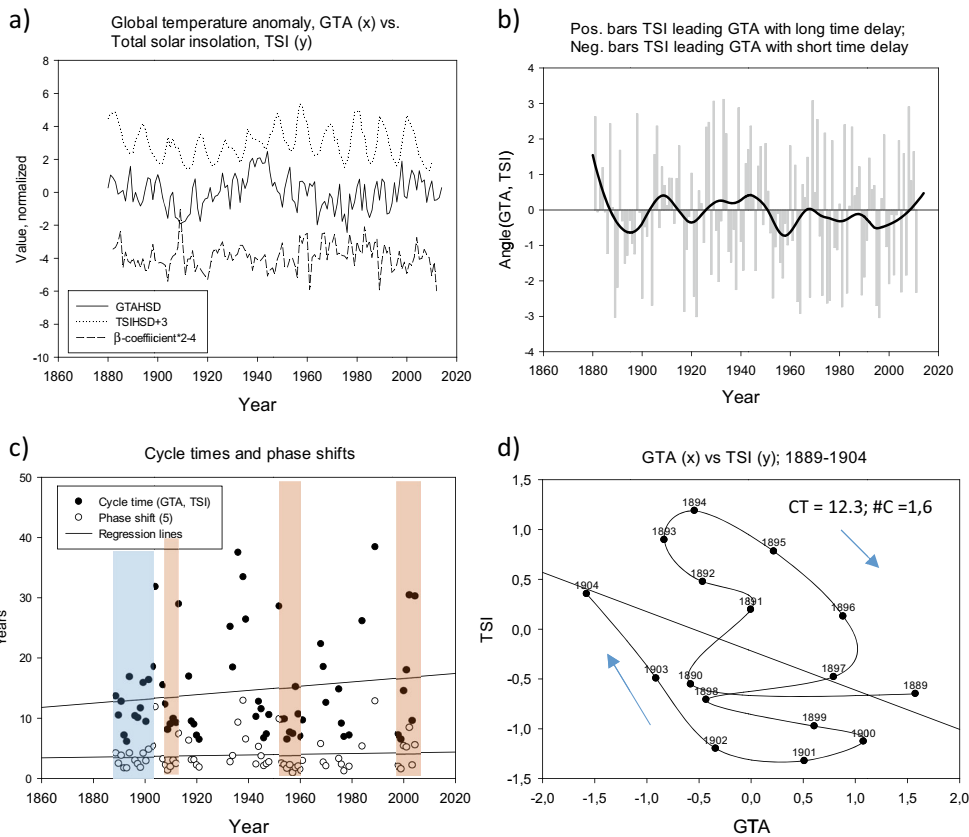
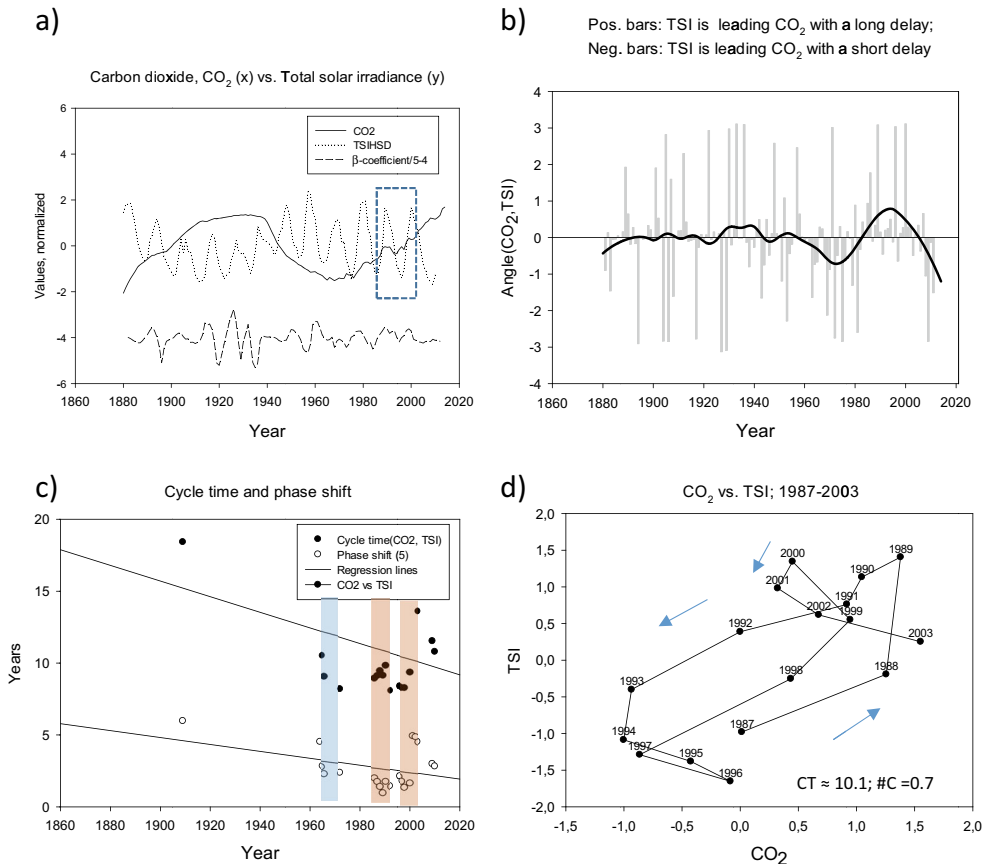


Fig. 6 Carbon dioxide (CO_2) versus total solar irradiance (*TSI*). **a** Time series for CO_2 (*full line*), and *TSI* (*dotted line*), *lower line* shows β -coefficient. Period 1880 to 2010. *Dotted square* indicates section where CO_2 apparently leads *TSI*. **b** Short and long leading times for *TSI* on CO_2 and *TSI*. *Positive bars* shows that *TSI* is leading CO_2 with a long time delay, PS_{long} ($>1/2$ cycle time, *CT*; i.e., $CT-PS_{short}$) and *negative bars* show that *TSI* is leading CO_2 with short time delay. The *full line* show smoothed trends in the LL-relationship (LOESS, $f=3, p=2$). **c** Running average cycle times (*CT*, *filled circles*, $n=9$) and phase shifts (*PS*, *open circles*, $n=5$) when both are significant, $p < 0.05$. **d** Phase diagram with CO_2 , (*x-axis*) and *TSI* (*y-axis*) for the years 1987 to 2003 (the period 1960 to 2003 detrended separately). Further details in text to Fig. 4



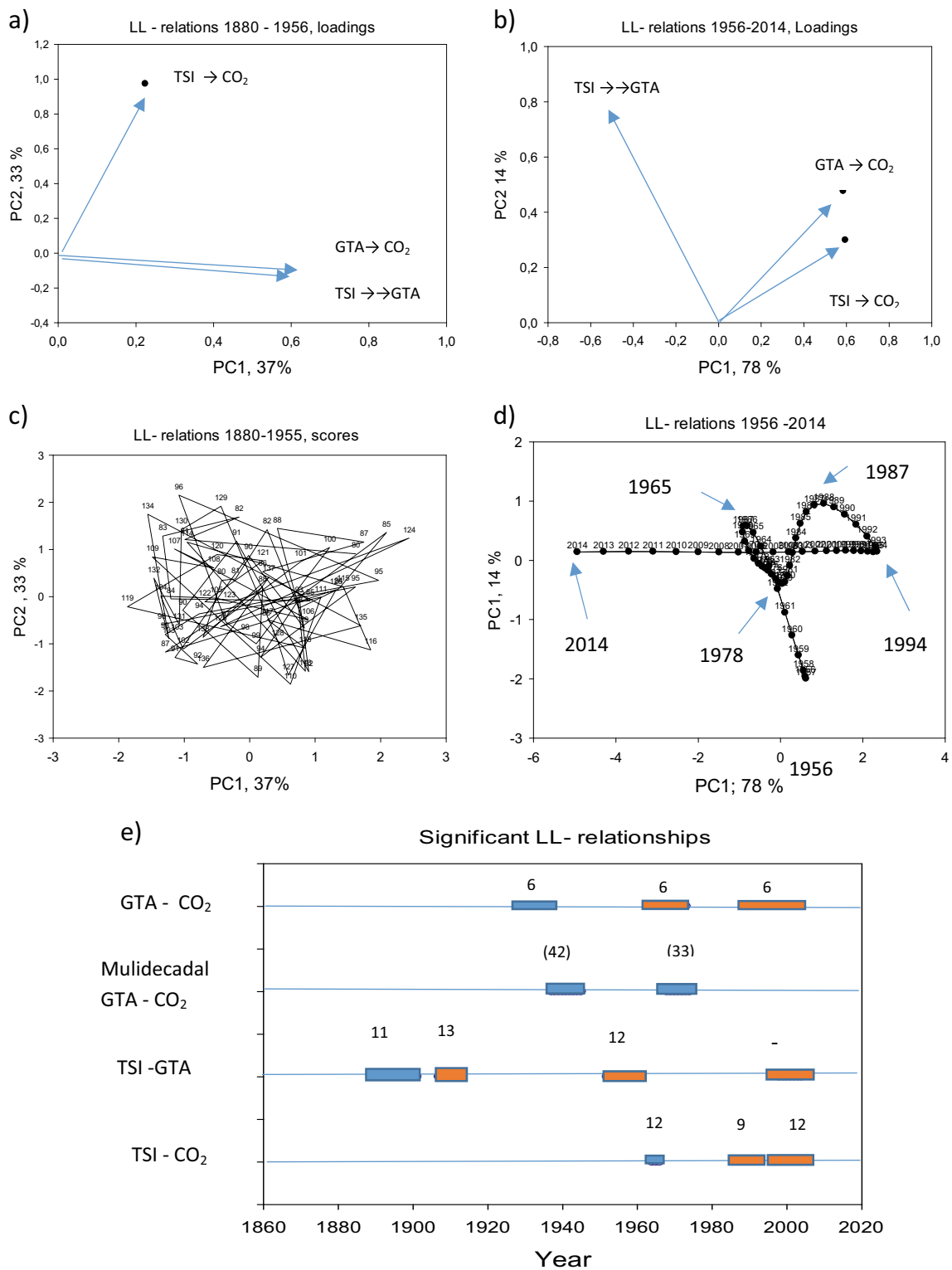


Fig. 7 Principal component plot for two periods (1880–1955 and 1956–2014) of leading-lagging (LL) relations between global temperature anomaly, carbon dioxide concentrations, and total solar irradiance: GTA-CO₂, TSI-GTA, and TSI-CO₂. Positive values of the interaction measure correspond to the directions shown in the legends. **a** Loading plot for the period 1880 to 1955. **b** Loading plot for the period 1956 to 2014. **c** Score plot for the period 1880 to 1955. **d** Score plot for the period

1956 to 2014. **e** Cycle times and significant LL-relationships. Double arrows indicate that time lags are long (>½ cycle time) Upper line: blue, CO₂ → GTA; red, GTA → CO₂; second line: blue, multidecadal CO₂ → multidecadal GTA (parentheses show that the numbers are only indicative). Third line: blue, TSI → GTA; red, TSI →→ GTA; fourth line: blue, TSI → CO₂; red, TSI →→ CO₂.

recognized in panels (b) of Figs. 4, 5, and 6. A PCA score plot for the full data set showed a pattern that defines the same years as in Fig. 7c as “turning” points (figure not shown). Time windows where pairs of time series show persistent LL-relationships are summarized in Table 1 and shown graphically in Fig. 7e.

4.5 Secular trends

The quadratic approximations to GTA, CO₂, and TSI are given below as Eqs. (14), (15), and (16). *T* is time in years starting with 1 in 1880. The number of observations, *n*, will differ a little among series depending upon the number of observations reported in the data sources.

$$GTA = -24.608 - 0.283 T + 0.00701 T^2; r = 0.770, p_1 = < 0.001, p_2 < 0.001, n = 135, \tag{14}$$

$$CO_2 = 2.99.429 - 0.326 T + 0.00741 T^2; r = 0.86, p_1 = 0.001, p_2 < 0.001, n = 135, \tag{15}$$

$$TSI = -0.0773 + 0.00430 T - 0.0000170 T^2, r = 0.67, p_1 < 0.001, p_2 < 0.001, n = 131. \tag{16}$$

The CO₂ and the GTA series decrease with time and increase with time squared, whereas the TSI series increase with time and decrease with time squared (Fig. 1b). This latter result is consistent with results reported by Frohlich (2009). Figure 1b also shows the LOESS trends as wiggling curves

fitting the observed curves more closely. The LOESS trend for CO₂ is monotonically increasing.

The explained variance between the independent variables CO₂ and TSI is *r*² = 0.33, thus allowing multiple regressions (Kleinbaum et al. 1988). MR is asymmetric in *x* and *y*. In terms of the native original time series, multiple regression gives:

$$GTA = -297.997 + 0.909 \times CO_2 + 35.816 \times TSI, R = 0.929, p_{CO_2} < 0.001; p_{TSI} = 0.006, n = 131 \tag{17}$$

In terms of smoothed, centered, and normalized data, we get:

$$GTA_{-N} = 0.00 + 0,916 \times CO_{2-N} + 0.101 TSI_{-N}, R = 0.989, p_{CO_2} < 0.001; p_{TSI} = 0.001, n = 135 \tag{18}$$

The results show that both trends in CO₂ and TSI contributed significantly to the changes of trends in GTA. If we do the calculation separately for the first and the last 30-year periods, GTA, we get contributions from CO₂ and TSI for the period 1910 to 1940 of 0.56 and 0.44 respectively and for the period 1970 to 2000 of 0.83 and 0.17 respectively. Using the revised data for GTA (Karl et al. 2015) and total sunspot numbers (Clette et al. 2014) from 2014, we get

$$GTA_{Karl} = 0.00 + 0,971 CO_2 + 0,0802 TSN_{Clette}, R = 0.990, p_{CO_2} < 0.001, P_{TSN} < 0.001, n = 135 \tag{19}$$

That is, no significant difference from the regression with the original data.

Table 1 Time windows where pairs of time series show persistent leading or lagging relations

Pair	Significant time windows, <i>n</i> > 3;	Significant, total, %	Cycle length, years	LL-relation	LL-times, years	# cycles	
GTA, CO ₂	1929–36 (*)	27	5.6	CO ₂ → GTA	1.6	−1.5	
	1966–73 (*)		6.4	GTA → CO ₂	1.5	+1.5	
	1989–03 (*)		5.3	GTA → CO ₂	1.2	+3.5	
GTA, CO ₂ , multidecadal	1937–45	12	(42)	CO ₂ → GTA	11.5	−0.24	
	1968–74		(33)	CO ₂ → GTA	9,6	−0.27	
TSI, GTA	1889–1901	56	11.4	TSI → GTA	3.1	−1.6	
	1907–13		13.4	TSI → → GTA	10.2	0.46	
	1943–48 (L.A.)		L.A.	L.A.	L.A.	L.A.	L.A.
	1952–61		11.9;	TSI → GTA	3.1	−1.4	
	1966–70 (L.A.)		L.A.	L.A.	L.A.	L.A.	L.A.
	1998–04		(16.7)	TSI → GTA	4.5	−0.2	
	1997–2005 (*)		12.0	TSI → → CO ₂	8.7	+0.7	
TSI; CO ₂	1964–66	15	(12.2)	TSI → CO ₂	3.2	−0.18	
	1986–92 (*)		9.1	TSI → → CO ₂	8	+0.8	
	1997–2005 (*)		12.0	TSI → → CO ₂	8.7	+0.7	

Years with asterisks shows windows that are intercepted with one non-significant year. L.A shows that there are very large angles, V, in the series that makes calculations of average cycle lengths not meaningful. Parentheses around cycle lengths show that only a small fraction of the cycle were sampled. Arrows suggest which variable leads and which follows. Double arrows indicate long (>1/2 cycle time) leading times

5 Discussion

Our aim with this study is to show the size of running average phase shifts and their direction between the variables global temperature anomaly (GTA), carbon dioxide concentration (CO₂), and total solar irradiance (TSI). The phase shifts we identify are interpreted in two ways. For paired variables that potentially may have reciprocal impact on each other, like CO₂ and GTA, we interpret the results in terms of leading and lagging relationships. For paired variables where one variable in the pair is exogenous to the system, we interpret results in terms of long (>½ cycle time) or short (<½ cycle time) delay times between the candidate leading variable as possible causal agent and the effect. However, there may be a variable that affects both the leading and the lagging variable, but the lagging variable later than the leading variable, e.g., temperature may affect the growth of two cohabiting species so that one peaks consistently before the other (Seip and Reynolds 1995). Finally, although we provide evidence for possible causal effects, credible mechanistic explanations are required to validate, or negate, causal relations.

The running average phase shift relations give additional information to relations found by ordinary regression analysis and may be useful in the search for mechanistic explanations of the cyclic components of global temperature changes. We first discuss our results for the cyclic components of our three variables, GTA, CO₂, and TSI. Thereafter, we discuss the results for the trends.

The leading lagging relations we found frequently contrast with our hypotheses. However, the 6- to 8-year cycles and the 9- to 11-year cycles that we found correspond with cycle times reported in the literature, e.g., Zhen-Shan and Xian (2007), p. 117–8 and Humlum et al. (2011), p. 151. We did not find the 20-year and the 60-year cycles reported in the literature, but the 60-year cycle is frequently associated with the North Atlantic oscillation (NOA) that is not included in the present study. We found that after about 1955, that is, in the middle of the period where there is little or negative changes in GTA, there is conspicuous changes in how the three variables interact.

5.1 Global temperature anomaly versus carbon dioxide

During the period 1929 to 1936, GTA was a lagging variable to CO₂, but after about 1955 (significant after 1966), GTA is a leading variable to CO₂, and the common cycle times are on the average 6.8 ± 2.0 years, leading, and lagging times 1.7 ± 0.8 years. This last period contrasts with our first hypothesis that CO₂ would be a leading variable to GTA also in their cyclic component. We do not believe that the results are caused by errors in the data since the result are for the period after 1945–1947 when data quality was improved. The two periods correspond with a reported low ocean CO₂ uptake flux

1901 to 1930 ($0.47 \text{ Pg C year}^{-1}$) to high uptake fluxes 1960 to 2005 ($1.53 \text{ Pg C year}^{-1}$) found in the CMIP5Earth System Model. During the same two periods, the mean land–atmosphere CO₂ fluxes changed from a small source for the atmosphere to a CO₂ sink during the last period (Anav et al. (2013), pp. 6817 and 6826 and Stocker (2014), p. 792).

Cycle lengths of 6 to 8 years The cycle times we found correspond well with the cycle times of 6 to 8 years reported by Zhen-Shan and Xian (2007), p. 118, using an empirical decomposition method (EMD) for global temperature anomaly. Cycle times and leading-lagging relations can also be seen visually (but not easily) by comparing time series sequences and phase plot trajectories for the periods where LL-relations are significant, e.g., 1990 to 2003 in Fig. 4a–d. For the smoothed GTA/CO₂ series (Fig. 4e, f), CO₂ is leading GTA. We found only short significant periods for common cycles lengths, but GTA has a visually distinct cycle of 60 years, and the detrended CO₂ a distinct third-order polynomial form (100 years “dome”) at the beginning of our study period. There are several studies that try to explain the identified cycle lengths in GTA time series, for example Keeling and Whorf (1997) invoke oceanic tides, whereas Ray (2007) and Munk et al. (2002) assess tides as the most likely among unlikely mechanisms. However, there are demonstrations, *sensu* Crick (1988), that could help explain cycle lengths. On a global scale, it is shown that CO₂ may escape from the oceans (Martinez-Boti et al. 2015), although these authors refer to intensified ocean upwelling during the deglaciation period (18,000 to 10,000 years ago), whereas Ray (2007), p. 3553 suggests that only shallow thermohaline circulations will contribute. Other studies suggest that there are regional oscillations in ocean waters, e.g., the Atlantic Multidecadal Oscillation (AMO) (Chylek et al. 2014a) and the (deep >750 m) interdecadal Pacific Oscillations (Meehl et al. 2013), that may give rise to regional and global temperature changes. Meehl et al. (2011) use the expression “The model provides a plausible.” p. 362, suggesting that the results have some uncertainty. The 60-year cycle in GTA has again been linked to a solar-astronomical origin by Mazzarella and Scafetta (2012). Recently, Finlay et al. (2015) have shown that there is a decrease in CO₂ efflux on a regional scale from northern hardwater lakes with increasing atmospheric warming.

Leading and lagging times Our leading lagging times are of the order 1 to 3 years. This contrasts with the fairly short time lags (months) reported by, e.g., Foster and Rahmstorf (2011), p. 6. We have identified three exceptions where lag correlation up to 12 years have been reported. Chylek et al. (2014a), p. 126 and Wu et al. (2011a) show a 12-year lag for the AMO/Pacific decadal oscillation system (there may be other explanations for the apparent lag). McCarthy et al. (2015) reported

that the integrated NAO lags their integrated sea-level index (related to heath transport) with 1–2 years, see text to their extended data (Fig. 7). We believe that the response times between CO₂ and GTA most probably are shorter than ½ cycle length, that is <3–4 years. For example, Feldman et al. (2015), p. 342 show that 1-year cycles of surface radiative forcings (Wm⁻²) by CO₂ may be due to seasonal changes in photosynthesis and respiration.

The cycle lengths identified for multidecadal cycles in Fig. 4f were based on less than ¼ cycle length and on averaged data where noise and end-effects may have distorted the results, and are therefore highly uncertain.

5.2 Global temperature anomaly and total solar irradiance

TSI is leading GTA with a short delay (< ½ cycle length) during three periods, but is a leading variable to GTA with a long delay (> ½ cycle length) during the period 1907–1913. Characteristic cycle times are 11 to 13 years corresponding to the cycle lengths for TSI, (the last period in Table 1 only allowed sampling of a very short cycle fraction). Short time lags were around 3 years and long time lags around 10 years. With long time lags, the peak in TSI is closer to the preceding peak in GTA than to the peak following it. For TSI to contribute a causal element, there should be modifying factors that delay the effect of TSI on GTA.

Indications for cycle times of 10–13 years and time lags An attempt to explain the 11 years response of the climate system to small solar cycle forcings was given in Meehl et al. (2009). Time lags between TSI and target variables are found in several studies. For the period 2004–2007, a delay between solar activity and radiative forcings >3 years was found by Haigh et al. (2010) and discussed further by Wen et al. (2013) and Ineson et al. (2015). It was attributed to a shift in dominant wavelengths of the emitted radiation. Furthermore, Andrews et al. (2015), p. 3 found a time lag for the, DJF (December, January, February) North Atlantic oscillation to the Upper stratospheric zonal temperature of 3 to 4 years. Solheim et al. (2012) found that there is a lag of about 10 years between solar cycle length and the 11 years average temperature at several stations in the North Atlantic. Thus, both short- and long-term delays may not be unreasonable. An alternative may be that the observed 9- to 10-year cycles are due to other variables than TSI, and that these variables produce cycles in the same range.

5.3 Carbon dioxide versus total solar irradiance

We found that TSI was leading CO₂ with a short delay during the period 1960 to 1980 (significant years in Table 1), but that TSI was leading CO₂ with a long delay during the period 1986

to 2005 (significant years in Table 1) (Fig. 6b). Common cycle times were 9 to 12 years corresponding to the typical cycle period reported for TSI (11.1 ± 1.2 years). The LL-relationships can be seen in both the time series (Fig. 6a) and in the phase plot (Fig. 6d). The figures also suggest that smoothing the trajectories in the phase plots may give more consistent rotation patterns. (See Supplementary material 2 for an example.) For the long delays, there must be modifying factors and they may partly be the same as those modifying the effect of TSI on GTA. We are presently examining phase shifts between GTA, NAO, SOI, and PDO, to see if these variables may contribute to an explanation.

5.4 Significant time windows

Our second hypothesis was that distinguishable common cycle times for paired variables would occur during different time windows. However, this does not seem to be the case, or at least our material does not give sufficient information to draw conclusions (Fig. 7e). Still, the years around 1955, that is, in the middle of the period with no, or little, global warming, seem to separate two warming regimes as suggested in Fig. 7a–d. (The year 1994 also suggests a change, but the period after 1994 is short and end-effects may play a role.) The results are only tentative, and we have no mechanistic explanation for why there would be two regimes, except that the CO₂ concentration has increased considerably after 1955. If the increased CO₂ concentration, or some other factor, triggered a new regime, the suggestion that the 60-year cycle in GTA will continue unchanged, which was implied by Zhen-Shan and Xian (2007), p. 118 and Chylek et al. (2014 a), p. 127, may not be as certain as previously believed.

5.5 Secular periods

The period 1880 to 2009 The results for the long-term trend suggest that both CO₂ and annual sunspot composite, TSI, have a significant impact on GTA, CO₂ being responsible for ≈90 % of changes in GTA, and TSI being responsible for ≈10 % using the coefficients in front of the regressors in Eq. (18) the β-coefficients, as a measure of how much of the signals, and probable causes, that are drawn from the two agents. The results can be compared to regression results by Chylek et al. (2014a), p. 122 who found that greenhouse gases account for 48 %, the Atlantic multidecadal oscillation for 40 %, and TSI for 12 % of the past US South Western temperatures (using again the normalized coefficients in front of the regressors).

Thus, our third hypothesis was supported, the shape of the trends for CO₂ (≈90 %) and TSI (≈10 %) contributes to changes in the trend for GTA. However, the contribution from the sun has decreased relative to the contribution from CO₂ during the last 135 years. Our results are novel in the sense

that they were obtained with methods applied to LOESS detrended data normalized to unit standard deviation, and thus show that we get results similar to current estimates without recalculating data to a common unit for radiative forcings, e.g., Wm⁻². We obtained similar results using new GTA data from Karl et al. (2015) and new proxies for TSI, that is, new total sunspot numbers from Clette et al. (2014).

5.6 Method

The present paper supplies a method that allows calculation of running average phase shifts, as well as running average cycle times. The method gives results that are not affected by changes in cycle lengths, and it detects single outliers in series that else would show consistent phase shift relationships. We have also used it to establish the length of periods that are characterized by consistent phase shifts between pairs of variables. Since the method is novel, it is important to establish that it does not give spurious or misleading results. We give four rationales for why its results are real. (i) The method has previously been shown to give significant LL-strength for relationships where leading relations belong to “common knowledge”, e.g., to leading indices in economy (Seip and McNown 2007) and to light as a leading variable to sea surface temperature in hydrobiology (Seip 2015). Light is a proxy for heat transfer. (ii) It is in many instances possible to inspect the paired series visually and to see from the cyclic pattern of the series that the variable which is identified as leading indeed is indeed a leading variable, e.g., as in Fig 6a. (iii) We show that for time windows where LL-relations are persistently leading or lagging, the corresponding phase portraits also rotate persistently clockwise or counterclockwise. (iv) We have applied the method to synthetic series and shown that it reproduces the design parameters well (see Supplementary material 1). Noise and interlocking cycles with different LL-relations and different cycle lengths may distort the results, in particular for cycle times. However, if persistent cycles can be identified in the phase plot, like they do here, the results are robust also with respect to cycle lengths and phase shifts based on unsmoothed series. An additional support for our results is that they changed a little, but not much, when GTA were replaced with an updated series (Karl et al. 2015), and TSI were replaced with total sunspot numbers as a proxy for TSI (Clette et al. 2014). However, a robust smoothing algorithm that does not introduce end-effects, or some way of subtracting high-frequency cycles from low-frequency cycles, remains a challenge.

6 Conclusion

We have obtained two sets of results, firstly on the cyclic components of the variables GTA, CO₂, and TSI and secondly

on their trends. We show that there are time windows where there are significant leading-lagging relationships between pairs of variables, and that the common cycle lengths we identify for the paired variables correspond to cycle lengths found in the literature, i.e., 6–7 and 10–11 years. We show that there are time windows where the causal variable comes (i.e., peak) more than half a cycle length before the effect variable (peaks). This suggests that there are strong roles for intermediate mechanisms in the global sea, land, and atmospheric system. These mechanisms may have changed during the period 1940–1970 when GTA was non-increasing, resulting in another interaction regime between the variables. Secondly, the trends in CO₂ and TSI seem to contribute approximately 90 and 10 % to the trend in GTA, respectively, during the last 130 years. However, TSI contributed relatively more (≈50 %) during the first 30 years, than during the last 30 years (<20 %) of our study period.

Acknowledgments We would like to thank Robert McNown for pointing out important literature for this study and for help in developing the leading-lagging ideas for climate studies. We thank Hans Martin Seip for pointing out relevant literature and for giving us useful comments and advices and Jostein-Riiser Kristiansen for providing the reference to Kjeldseth-Moe and Wedenmeyer-Böhm (2009). We would also like to thank two anonymous referees for constructive criticism and helpful comments. All data are available from the sources cited in the materials section of the paper, but are also supplied in Excel format as supporting information.

References

- Anav A, Friedlingstein P, Kidston M, Bopp L, Ciais P, Cox P, Jones C, Jung M, Myneri R, Zhu Z (2013) Evaluating the land and ocean components of the global carbon cycle in the CMIP5 earth system models. *J Clim* 26(18):6801–6843
- Andrews MB, Knight JR, Gray LJ (2015) A simulated lagged response of the north Atlantic oscillation to the solar cycle over the period 1960–2009. *Environ Res Lett* 10(5)
- Bacastow RB (1976) Modulation of atmospheric carbon dioxide by the southern oscillation. *Nature* 261:116–118
- Chylek P, Dubey MK, Lesins G, Li JN, Hengartner N (2014a) A. Imprint of the Atlantic multi-decadal oscillation and Pacific decadal oscillation on southwestern US climate: past, present, and future. *Clim Dyn* 43(1–2):119–129
- Chylek P, Klett JD, Lesins G, Dubey MK, Hengartner N (2014b) b). The Atlantic multidecadal oscillation as a dominant factor of oceanic influence on climate. *Geophys Res Lett* 41(5):1689–1697
- Clette F, Svalgaard L, Vaquero JM, Cliver EW (2014) Revisiting the sunspot number a 400-year perspective on the solar cycle. *Space Sci Rev* 186(1–4):35–103
- Cooley, T. F. and E. C. Prescott (1995). Economic growth and business cycles (Chapt. 1.). *Frontiers of business cycle research*. T. F. Cooley. Princeton, Princeton university press: 1–38.
- Crick FHC (1988) What mad pursuit. A personal view of scientific discovery. Basic Books, Inc, New York
- DelSole T, Tippett MK, Shukla J (2011) A significant component of unforced multidecadal variability in the recent acceleration of global warming. *J Clim* 24(3):909–926

- Feldman DR, Collins WD, Gero PJ, Tom MS, Mlawer EJ, Shippert TR (2015) Observational determination of surface radiative forcing by CO₂ from 2000 to 2010. *Nature* 519(7543):339 – +
- Finlay K, Vogt RJ, Bogard MJ, Wissel B, Tutolo BM, Simpson GL, Leavitt PR (2015) Decrease in CO₂ efflux from northern hardwater lakes with increasing atmospheric warming. *Nature* 519(7542):215–218
- Foster G, Rahmstorf S (2011) Global temperature evolution 1979–2010. *Environ Res Lett* 6:8
- Fröhlich C (2009) Evidence of a long-term trend in total solar irradiance. *Astronomy & Astrophysics* 501(3):L27–U508
- Gao LH, Yan ZW, Quan XW (2015) Observed and SST-forced multidecadal variability in global land surface air temperature. *Clim Dyn* 44(1–2):359–369
- Haigh JD, Winning AR, Toumi R, Harder JW (2010) An influence of solar spectral variations on radiative forcing of climate. *Nature* 467(7316):696–699
- Humlum O, Solheim JE, Stordahl K (2011) Identifying natural contributions to late Holocene climate change. *Glob Planet Chang* 79(1–2): 145–156
- Ineson S, Maycock AC, Gray LJ, Scaife AA, Dunstone NJ, Harder JW, Knight JR, Lockwood M, Manners JC, Wood RA (2015) Regional climate impacts of a possible future grand solar minimum. *Nat Commun* 6. doi:10.1038/ncomms8535
- Karl TR, Arguez A, Huang BY, Lawrimore JH, McMahon JR, Menne MJ, Peterson TC, Vose RS, Zhang HM (2015) Possible artifacts of data biases in the recent global surface warming hiatus. *Science* 348(6242):1469–1472
- Keeling CD, Whorf TP (1997) Possible forcing of global temperature by oceanic tides. *Proc Natl Acad Sci U S A* 94:8321–8328
- Kjeldseth-Moe O, Wedenmeyer-Böhm S (2009) Are there variations in earth's global mean temperature related to the solar activity? Impact on Earth and Planets, International Astronomical Union, Solar and Stellar Variability
- Kleinbaum DG, Kupper LL, Muller KE (1988) Applied regression analysis and other multivariate methods. PES-KENT publishing company, Boston
- Luterbacher J, Koplaki E, Dietrich D, Rickli R, Jacobeit J, Beck C, Gyalistras D, Schmutz C, Wanner H (2002) Reconstruction of sea level pressure fields over the eastern north Atlantic and Europe back to 1500. *Clim Dyn* 18(7):545–561
- Martinez-Boti MA, Marino G, Foster GL, Ziveri P, Henehan MJ, Rae JWB, Mortyn PG, Vance D (2015) Boron isotope evidence for oceanic carbon dioxide leakage during the last deglaciation. *Nature* 518(7538):219–U154
- Mazzarella A, Scafetta N (2012) Evidences for a Quasi 60-year north Atlantic oscillation since 1700 and its meaning for global climate change. *Theor Appl Climatol* 107(3–4):599–609
- McCarthy GD, Haigh ID, Hirschi JIJ-M, Grist JP, Smeed DA (2015) Ocean impact on decadal Atlantic climate variability revealed by sea-level observations. *Nature* 521:508–510. doi:10.1038/nature14491
- Meehl GA, Arblaster JM, Fasullo JT, Hu AX, Trenberth KE (2011) Model-based evidence of deep-ocean heat uptake during surface-temperature hiatus periods. *Nat Clim Chang* 1(7):360–364
- Meehl GA, Arblaster JM, Matthes K, Sassi F, van Loon H (2009) Amplifying the Pacific climate system response to a small 11-year solar cycle forcing. *Science* 325(5944):1114–1118
- Meehl GA, Hu AX, Arblaster JM, Fasullo J, Trenberth KE (2013) Externally forced and internally generated decadal climate variability associated with the interdecadal Pacific oscillation. *J Clim* 26(18):7298–7310
- Meehl GA, Teng HY, Arblaster JM (2014) Climate model simulations of the observed early-2000s hiatus of global warming. *Nat Clim Chang* 4(10):898–902
- Munk W, Dzieciuch M, Jayne S (2002) Millennial climate variability: is there a tidal connection? *J Clim* 15(4):370–385
- NASA(GHG). (2014). Greenhouse gases and Total solar irradiance. from <http://data.giss.nasa.gov/modelforce/RadF.txt>
- NASA(GISTEMP). (2014). GISS Surface Temperature Analysis (GISTEMP). 2012, from <http://data.giss.nasa.gov/gistemp>
- Power SB, Kociuba G (2011) What caused the observed twentieth-century weakening of the walker circulation? *J Clim* 24(24):6501–6514
- Ray RD (2007) Decadal climate variability: is there a tidal connection? *J Clim* 20(14):3542–3560
- Ring MJ, Lindner D, Cross E, Schlesinger FME (2012) Causes of the global warming observed since the 19th century. *Atmospheric and Climate sciences* 2:401–415
- Seip KL (2015) Investigating possible causal relations among physical, chemical and biological variables across regions in the gulf of Maine. *Hydrobiologia* 744:127–143
- Seip KL, McNown R (2007) The timing and accuracy of leading and lagging business cycle indicators: a new approach. *Int J Forecast* 22: 277–287
- Seip KL, Pleym H (2000) Competition and predation in a seasonal world. *Verh Internat Verein Limnol* 27:823–827
- Seip KL, Reynolds CS (1995) Phytoplankton functional attributes along trophic gradient and season. *Limnol Oceanogr* 40:589–597
- Solheim JE, Stordahl K, Humlum O (2012) The long sunspot cycle 23 predicts a significant temperature decrease in cycle 24. *J Atmos Sol Terr Phys* 80:267–284
- SORCE (2015) Total solar irradiance data. <http://lasp.colorado.edu/home/sorce/data/tsi-data/>
- Stocker, T. (2014). Climate change 2013 : the physical science basis : Working Group I contribution to the Fifth assessment report of the Intergovernmental Panel on Climate Change. Cambridge university press
- Wen GY, Cahalan RF, Haigh JD, Pilewskie P, Oreopoulos L, Harder JW (2013) Reconciliation of modeled climate responses to spectral solar forcing. *J Geophys Res-Atmos* 118(12):6281–6289
- White WB, Cayan DR (1998) Quasi periodicity and global symmetries in interdecadal upper ocean temperature variability. *J Geophys Res* 103:21335–21354
- Wu S, Liu ZY, Zhang R, Delworth TL (2011b) On the observed relationship between the Pacific decadal oscillation and the Atlantic multi-decadal oscillation. *J Oceanogr* 67(1):27–35
- Wu ZH, Huang NE, Wallace JM, Smoliak BV, Chen XY (2011a) On the time-varying trend in global-mean surface temperature. *Clim Dyn* 37(3–4):759–773
- Zhen-Shan L, Xian S (2007) Multi-scale analysis of global temperature changes and trend of a drop in temperature in the next 20 years. *Meteorog Atmos Phys* 95(1–2):115–121
- Zhou J, Tung K-K (2010) Solar cycles in 150 years of global sea surface temperature data. *J Clim* 23:3234–3248